Inorg. Chem. **2005**, *44*, 8810–8821

Correlation of Spin States and Spin Delocalization with the Dioxygen Reactivity of Catecholatoiron(III) Complexes

Masakazu Higuchi,[†] Yutaka Hitomi,*[,†] Hisataka Minami,[†] Tsunehiro Tanaka,[†] and Takuzo Funabiki*[,‡]

Department of Molecular Engineering, Graduate School of Engineering, Kyoto University, Katsura, Nishikyo-ku, Kyoto 615-8510, Japan, and Biomimetics Research Center, Doshisha University, Kyo-Tanabe, Kyoto 610-0321, Japan

Received July 13, 2005

A series of catecholatoiron(III) complexes, $[Fe^{III}L(4Cl\text{-}cat)]BPh_4$ (L = $(4\text{-}MeO)_2$TPA (**1**), TPA (**2**), $(4\text{-}Cl)_2$TPA (**3**), $(4\text{-}NO_2)$TPA (**4**), $(4\text{-}NO_2)_2$TPA (**5**); TPA = tris(pyridin-2-ylmethyl)amine; 4Cl-cat = 4-chlorocatecholate), have been characterized by magnetic susceptibility measurements and EPR, ^{1}H NMR, and UV–vis–NIR spectroscopies to clarify the correlation of the spin delocalization on the catecholate ligand with the O_2 reactivity as well as the spin-state dependence of the O_2 reactivity. EPR spectra in frozen CH_3CN at 123 K clearly showed that introduction of electron-withdrawing groups effectively shifts the spin equilibrium from a high-spin to a low-spin state. The effective magnetic moments determined by the Evans method in a CH_3CN solution showed that **5** contains 36% of low-spin species at 243 K, while **1**–**4** are predominantly in a high-spin state. Evaluation of spin delocalization on the 4Cl-cat ligand by paramagnetic ^{1}H NMR shifts revealed that the semiquinonatoiron(II) character is more significant in the low-spin species than in the high-spin species. The logarithm of the reaction rate constant is linearly correlated with the energy gap between the catecholatoiron(III) and semiquinonatoiron(II) states for the high-spin complexes **1**–**3**, although complexes **4** and **5** deviate negatively from linearity. The lower reactivity of the low-spin complex, despite its higher spin density on the catecholate ligand compared with the high-spin analogues, suggests the involvement of the iron(III) center, rather than the catecholate ligand, in the reaction with O_2.

Introduction

Catechol dioxygenases are mononuclear nonheme enzymes playing a key role in the metabolism of aromatic compounds such as lignin and halogenated benzene in soil bacteria.[1−4] They catalyze the C−C bond cleavage of the catechol ring and are subclassified into two classes: intradiol and extradiol catechol dioxygenases. Intradiol catechol dioxygenases utilize an Fe^{III} ion as an active center, whereas extradiol catechol dioxygenases require an Fe^{II} ion or rarely a Mn^{II} ion. In intradiol oxygenases, the Fe^{III} ion is ligated by two tyrosine and two histidine residues and water (OH^-) in a distorted trigonal bipyramidal geometry.[5−9] The two tyrosine residues are thought to play a role in lowering the redox potential to prevent the reduction of the ferric center under biological conditions.[10] When catechol coordinates to the Fe^{III} center in a chelate fashion, one tyrosine residue is released to form a distorted octahedral geometry bearing a vacant site. This intermediate species reacts with O_2 to give an intradiol-cleaving product, *cis*,*cis*-muconic acid. It is noteworthy that the active site iron retains the high-spin ferric oxidation state during the catalytic cycle.[10−17]

Functional model complexes for catechol oxygenases have been developed for evaluation of the reaction mechanisms and development of catalytic systems for catechol oxygena-

* To whom correspondence should be addressed. E-mail: hitomi@moleng.kyoto-u.ac.jp.
[†] Kyoto University.
[‡] BMRC, Doshisha University.

(1) Funabiki, T. *Dioxygenases*; Funabiki, T., Ed.; Kluwer Academic Publishers: Dordrecht, The Netherlands, 1997; pp 19−104.
(2) Bugg, T. D. H.; Winfield, C. J. *Nat. Prod. Rep.* **1998**, *15*, 513−530.
(3) Solomon, E. I.; Brunold, T. C.; Davis, M. I.; Kemsley, J. N.; Lee, S. K.; Lehnert, N.; Neese, F.; Skulan, A. J.; Yang, Y. S.; Zhou, J. *Chem. Rev.* **2000**, *100*, 235−349.
(4) Costas, M.; Mehn, M. P.; Jensen, M. P.; Que, L., Jr. *Chem. Rev.* **2004**, *104*, 939−986.
(5) Ohlendorf, D. H.; Lipscomb, J. D.; Weber, P. C. *Nature* **1988**, *336*, 403−405.
(6) Ohlendorf, D. H.; Orville, A. M.; Lipscomb, J. D. *J. Mol. Biol.* **1994**, *244*, 586−608.
(7) Vetting, M. W.; Ohlendorf, D. H. *Structure (Cambridge, MA)* **2000**, *8*, 429−440.
(8) Vetting, M. W.; D'Argenio, D. A.; Ornston, L. N.; Ohlendorf, D. H. *Biochemistry* **2000**, *39*, 7943−7955.
(9) Ferraroni, M.; Solyanikova, I. P.; Kolomytseva, M. P.; Scozzafava, A.; Golovleva, L.; Briganti, F. *J. Biol. Chem.* **2004**, *279*, 27646−27655.
(10) Pyrz, J. W.; Roe, A. L.; Stern, L. J.; Que, L., Jr. *J. Am. Chem. Soc.* **1985**, *107*, 614−620.

10.1021/ic051173y CCC: $30.25
Published on Web 10/13/2005

tions.[4,18−22] In the reaction of catecholatoiron(III) complexes with O_2, the importance of participation of the semiquinonatoiron(II) form has been proposed[19,23,24] and supported by various experimental[25−31] and theoretical results.[32,33] It was suggested that the ground state of the catecholatoiron(III) complexes is represented as a quantum mechanical admixture of Fe^{III}−Cat and Fe^{II}−SQ states, rather than an equilibrium between them.[25,27,28,34] On the basis of this Fe^{II}−SQ character of the Fe^{III}−Cat complex, two different paths have been proposed for the reaction with O_2 (Scheme 1); *path a*, *the substrate activation path*, is the one in which O_2 reacts first with the catechol moiety to give an Fe^{II}−R−OO$^{\bullet}$ form,[27,35−38] and *path b*, *the oxygen activation path*, is the one in which O_2 reacts first with an iron moiety to give an $^{\bullet}$OO−Fe^{III}−SQ form.[33,39] Path *a* has been favored, but data supporting path *b* has recently been obtained.[26,40,41]

Scheme 1. Two Possible Reaction Mechanisms for Intradiol Catechol Dioxygenases[a]

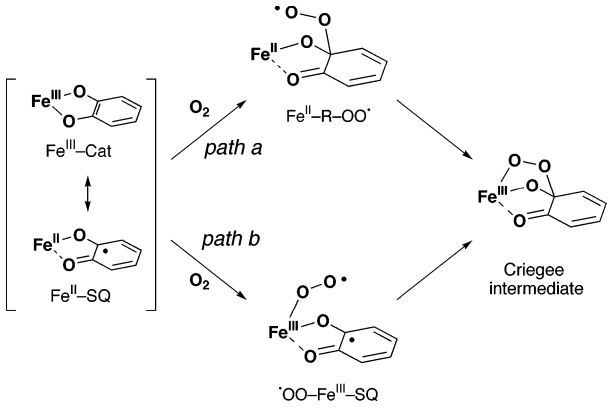

[a] Paths *a* and *b* show the substrate activation mechanism and the oxygen activation mechanism, respectively.

The iron(III) center of intradiol catechol dioxygenases is in a high-spin state, and the functional models so far developed also contain a high-spin ferric center at ambient temperatures.[22] However, the reactivity of low-spin catecholatoiron(III) complexes should provide valuable information on the reaction mechanism.[29] Recently, it has been shown that the spin state of catecholatoiron(III) complexes changes from high-spin to low-spin in the solid state with lowering temperatures[25,42,43] and that the substituents of the catecholate ligand greatly affect the spin-crossover transition.[25] The spin-crossover behavior has been well documented for ferric complexes with an N_4O_2 donor set in the solid state,[44−49] but it has been little documented in solution.[50,51]

We have synthesized a series of catecholatoiron(III) complexes, [Fe^{III}L(4Cl-cat)]BPh_4 (L = (4-MeO)$_2$TPA (**1**), TPA (**2**), (4-Cl)$_2$TPA (**3**), (4-NO_2)TPA (**4**), (4-NO_2)$_2$TPA (**5**)),[52] to investigate the substituent effects of the supporting ligand on spin delocalization and the O_2 reactivity.[53] It was found that the introduction of electron-withdrawing groups on the TPA ligand not only induces spin delocalization on

(11) Que, L., Jr.; Lipscomb, J. D.; Zimmermann, R.; Muenck, E.; Orme-Johnson, N. R.; Orme-Johnson, W. H. *Biochim. Biophys. Acta* **1976**, *452*, 320−334.
(12) Whittaker, J. W.; Lipscomb, J. D.; Kent, T. A.; Muenck, E. *J. Biol. Chem.* **1984**, *259*, 4466−4475.
(13) Kent, T. A.; Münck, E.; Pyrz, J. W.; Widom, J.; Que, L. *Inorg. Chem.* **1987**, *26*, 1402−1408.
(14) Que, L., Jr.; Heistand, R. H., II. *J. Am. Chem. Soc.* **1979**, *101*, 1, 2219−2221.
(15) Walsh, T. A.; Ballou, D. P.; Mayer, R.; Que, L., Jr. *J. Biol. Chem.* **1983**, *258*, 14422−14427.
(16) Bull, C.; Ballou, D. P.; Otsuka, S. *J. Biol. Chem.* **1981**, *256*, 2681−2686.
(17) Felton, R. H.; Cheung, L. D.; Phillips, R. S.; May, S. W. *Biochem. Biophys. Res. Commun.* **1978**, *85*, 844−850.
(18) Funabiki, T.; Sakamoto, H.; Yoshida, S.; Tarama, K. *J. Chem. Soc., Chem. Commun.* **1979**, 754−755.
(19) Funabiki, T.; Mizoguchi, A.; Sugimoto, T.; Tada, S.; Tsuji, M.; Sakamoto, H.; Yoshida, S. *J. Am. Chem. Soc.* **1986**, *108*, 2921−2932.
(20) Funabiki, T. *Iron Model Studies on Dioxygenases*; Funabiki, T., Ed.; Kluwer Academic Publishers: Dordrecht, The Netherlands, 1997; pp 105−156.
(21) Funabiki, T. *Functional Model Oxygenations by Nonheme Iron Complexes*; Simandi, L. I., Ed.; Kluwer: Dordrecht, The Netherlands, 2003; pp 157−226.
(22) Yamahara, R.; Ogo, S.; Masuda, H.; Watanabe, Y. *J. Inorg. Biochem.* **2002**, *88*, 284−294 and references therein.
(23) Funabiki, T.; Tada, S.; Yoshioka, T.; Takano, M.; Yoshida, S. *J. Chem. Soc., Chem. Commun.* **1986**, 1699−1700.
(24) Funabiki, T.; Konishi, T.; Kobayashi, S.; Mizoguchi, A.; Takano, M.; Yoshida, S. *Chem. Lett.* **1987**, 719−722.
(25) Funabiki, T.; Fukui, A.; Hitomi, Y.; Higuchi, M.; Yamamoto, T.; Tanaka, T.; Tani, F.; Naruta, Y. *J. Inorg. Biochem.* **2002**, *91*, 151−158.
(26) Hitomi, Y.; Yoshida, M.; Higuchi, M.; Minami, H.; Tanaka, T.; Funabiki, T. *J. Inorg. Biochem.* **2005**, *99*, 755−763.
(27) Cox, D. D.; Que, L., Jr. *J. Am. Chem. Soc.* **1988**, *110*, 8085−8092.
(28) Jang, H. G.; Cox, D. D.; Que, L., Jr. *J. Am. Chem. Soc.* **1991**, *113*, 9200−9204.
(29) Mialane, P.; Tchertanov, L.; Banse, F.; Sainton, J.; Girerd, J. J. *Inorg. Chem.* **2000**, *39*, 2440−2444.
(30) Viswanathan, R.; Palaniandavar, M.; Balasubramanian, T.; Muthiah, T. P. *Inorg. Chem.* **1998**, *37*, 2943−2951.
(31) Pascaly, M.; Duda, M.; Schweppe, F.; Zurlinden, K.; Muller, F. K.; Krebs, B. *Dalton Trans.* **2001**, 828−837.
(32) Funabiki, T.; Inoue, T.; Kojima, H.; Konishi, T.; Tanaka, T.; Yoshida, S. *J. Mol. Catal.* **1990**, *59*, 367−371.
(33) Funabiki, T.; Yamazaki, T. *J. Mol. Catal. A* **1999**, *150*, 37−47.
(34) Simaan, A. J.; Boillot, M.-L.; Carrasco, R.; Cano, J.; Girerd, J.-J.; Mattioli, T. A.; Ensling, J.; Spiering, H.; Gütlich, P. *Chem.*−*Eur. J.* **2005**, *11*, 1779−1793.
(35) Que, L., Jr.; Lipscomb, J. D.; Muenck, E.; Wood, J. M. *Biochim. Biophys. Acta* **1977**, *485*, 60−74.
(36) Que, L.; Kolanczyk, R. C.; White, L. S. *J. Am. Chem. Soc.* **1987**, *109*, 5373−5380.
(37) Que, L.; Lauffer, R. B.; Lynch, J. B.; Murch, B. P.; Pyrz, J. W. *J. Am. Chem. Soc.* **1987**, *109*, 5381−5385.
(38) Fujii, S.; Ohyanishiguchi, H.; Hirota, N.; Nishinaga, A. *Bull. Chem. Soc. Jpn.* **1993**, *66*, 1408−1419.
(39) Funabiki, T.; Kojima, H.; Kaneko, M.; Inoue, T.; Yoshioka, T.; Tanaka, T.; Yoshida, S. *Chem. Lett.* **1991**, 2143−2146.
(40) Jo, D.-H.; Que, L., Jr. *Angew. Chem., Int. Ed.* **2000**, *39*, 4284−4287.
(41) Hitomi, Y.; Tase, Y.; Higuchi, M.; Tanaka, T.; Funabiki, T. *Chem. Lett.* **2004**, *33*, 316−317.
(42) Simaan, A. J.; Boillot, M.-L.; Rivière, E.; Boussac, A.; Girerd, J.-J. *Angew. Chem., Int. Ed.* **2000**, *39*, 196−198.
(43) Floquet, S.; Simaan, A. J.; Rivière, E.; Nierlich, M.; Thuéry, P.; Ensling, J.; Gütlich, P.; Girerd, J. J.; Boillot, M. L. *Dalton Trans.* **2005**, 1734−1742.
(44) Haddad, M. S.; Lynch, M. W.; Federer, W. D.; Hendrickson, D. N. *Inorg. Chem.* **1981**, *20*, 123−131.
(45) Ohshio, H.; Maeda, Y.; Takashima, Y. *Inorg. Chem.* **1983**, *22*, 2684−2689.
(46) Timken, M. D.; Hendrickson, D. N.; Sinn, E. *Inorg. Chem.* **1985**, *24*, 3947−3955.
(47) Timken, M. D.; Strouse, C. E.; Soltis, S. M.; Daverio, S. A.; Hendrickson, D. N.; Abdelmawgoud, A. M.; Wilson, S. R. *J. Am. Chem. Soc.* **1986**, *108*, 395−402.
(48) Oshio, H.; Toriumi, K.; Maeda, Y.; Takashima, Y. *Inorg. Chem.* **1991**, *30*, 4252−4260.
(49) Boca, R.; Fukuda, Y.; Gembicky, M.; Herchel, R.; Jarosciak, R.; Linert, W.; Renz, F.; Yuzurihara, J. *Chem. Phys. Lett.* **2000**, *325*, 411−419.
(50) Wilson, L. J.; Tweedle, M. F. *J. Am. Chem. Soc.* **1976**, *98*, 4824−4833.
(51) Petty, R. H.; Dose, E. V.; Tweedle, M. F.; Wilson, L. J. *Inorg. Chem.* **1978**, *17*, 1064−1070.

the catecholate ligand but also shifts the spin equilibrium to a low-spin state. The logarithm of the reaction rate constant with O_2 is linearly correlated with the energy gap between catecholatoiron(III) and semiquinonatoiron(II) states for the high-spin complexes **1**−**3**, although **5**, which contains 36% of low-spin species at 243 K, deviates negatively from linearity. In this report, we elucidated the spin delocalization on the catecholate ligand of high-spin and low-spin catecholatoiron(III) species by means of ^{1}H NMR, EPR, and UV−vis−NIR spectroscopies to clarify the correlation of spin states and spin delocalization with the O_2 reactivity of catecholatoiron(III) complexes.

Experimental Section

Materials and Preparation of Ligands and Complexes. Reagents and solvents used were commercially available unless otherwise stated. 4Cl-catH_2 was purified by sublimation in vacuo. The TPA ligand, 2-chloromethyl-4-methoxypyridine, 4-chloro-2-chloromethylpyridine, and 2-chloromethyl-4-nitropyridine were prepared using the method reported previously.[54,55]

Synthesis of TPA Derivatives. Bis(4-methoxypyridin-2-ylmethyl)(pyridin-2-ylmethyl)amine, (4-MeO)$_2$TPA. 2-Chloromethyl-4-methoxypyridine (0.58 g, 3.7 mmol) and 10 N NaOH (aq) (0.8 mL, 8.0 mmol) were added to a stirred solution of 2-picolylamine (0.19 g, 1.8 mmol) in water (1 mL). The reaction mixture was stirred at room temperature for 3 days. The organic layer was separated, and the aqueous layer was extracted with CH_2Cl_2 several times. The combined organic layers were dried over Na_2SO_4, and the volatile components were removed. Purification of the crude product on an alumina column (3:1 AcOEt/CH_2Cl_2) gave 0.39 g (60%) of yellow oil. ^{1}H NMR (400 MHz, $CDCl_3$): δ 3.85 (6H, s), 3.86 (4H, s), 3.90 (2H, s), 6.67 (2H, dd, J = 5.9 Hz, J' = 2.4 Hz), 7.14 (1H, dd, J = 7.8 Hz, J' = 4.9 Hz), 7.20 (2H, d, J = 2.4 Hz), 7.56 (1H, d, J = 7.8 Hz), 7.64 (1H, ddd, J = 7.8 Hz, J' = 7.8 Hz J'' = 2.0 Hz), 8.34 (2H, d, J = 5.9 Hz), 8.53 (1H, dd, J = 4.9 Hz, J' = 2.0 Hz). ^{13}C NMR (100 MHz, $CDCl_3$): δ 55.1, 60.2, 60.3, 108.3, 108.6, 121.9, 122.9, 136.3, 149.0, 150.2, 159.2, 161.1, 166.1.

Bis(4-chloropyridin-2-ylmethyl)(2-pyridylmethyl)amine, (4-Cl)$_2$TPA. (4-Cl)$_2$TPA was prepared using 4-chloro-2-chloromethylpyridine in a manner analogous to that used to prepare (4-MeO)$_2$TPA; it was isolated as light yellow oil in a 66% yield. ^{1}H NMR (400 MHz, $CDCl_3$): δ 3.89 (4H, s), 3.91 (2H, s), 7.18−7.15 (3H), 7.51 (1H, d, J = 7.8 Hz), 7.56 (2H, d, J = 2.0 Hz), 7.68 (1H, ddd, J = 7.8 Hz, J' = 7.8 Hz, J'' = 2.0 Hz), 8.43 (2H, d, J = 5.4 Hz), 8.56 (1H, d, J = 4.4 Hz). ^{13}C NMR (100 MHz, $CDCl_3$): δ 59.9, 60.4, 122.2, 122.5, 123.0, 123.2, 136.5, 144.5, 149.1, 149.6, 158.5, 160.9.

Bis(pyridin-2-ylmethyl)(4-nitropyridin-2-ylmethyl)amine, (4-NO$_2$)TPA. (4-NO$_2$)TPA was prepared using 2,2′-dipicolylamine and 2-chloromethyl-4-nitropyridine (1:1) in a manner analogous to that used to prepare (4-MeO)$_2$TPA; it was isolated as light yellow oil in a 41% yield. ^{1}H NMR (400 MHz, $CDCl_3$): δ 3.94 (6H, s), 4.06 (2H, s), 7.16 (2H, dd, J = 7.3 Hz, J' = 4.9 Hz), 7.54 (2H, d, J = 7.3 Hz), 7.68 (2H, dd, J = 7.3 Hz, J' = 7.3 Hz), 7.84 (1H, dd, J = 5.4 Hz, J' = 2.4 Hz), 8.35 (1H, d, J = 2.4 Hz), 8.55 (2H, d, J = 4.9 Hz,), 8.79 (1H, d, J = 5.4 Hz). ^{13}C NMR (100 MHz, $CDCl_3$): δ 59.7, 60.5, 114.3, 115.3, 122.1, 123.0, 136.5, 149.1, 151.0, 154.3, 158.5, 163.7.

Bis(4-nitroypyridin-2-ylmethyl)(pyridin-2-ylmethyl)amine, (4-NO$_2$)$_2$TPA. (4-NO$_2$)$_2$TPA was prepared using 4-chloro-2-nitromethylpyridine in a manner analogous to that used to preprare (4-MeO)$_2$TPA; it was isolated as light yellow oil in a 66% yield. ^{1}H NMR (400 MHz, $CDCl_3$): δ 3.98 (2H, s), 4.12 (4H, s), 7.12 (1H, ddd, J = 7.3 Hz, J' = 4.9 Hz, J'' = 1.0 Hz), 7.49 (1H, dd, J = 7.3 Hz, J' = 1.0 Hz), 7.69 (1H, ddd, J = 7.3 Hz, J' = 7.3 Hz, J'' = 1.0 Hz), 7.88 (2H, dd, J = 5.4 Hz, J' = 2.0 Hz), 8.31 (2H, d, J = 2.0 Hz), 8.57 (1H, dd, J = 4.9 Hz, J' = 1.0 Hz), 8.84 (2H, d, J = 5.4 Hz). ^{13}C NMR (100 MHz, $CDCl_3$): δ 59.9, 60.6, 114.6, 115.5, 122.4, 123.1, 136.6, 149.3, 151.3, 154.3, 157.9, 162.8.

General Procedure for the Synthesis of Catecholatoiron(III) Complexes. Substituted TPA (0.30 mmol) in methanol (2 mL) and 4Cl-catH_2 (0.043 g, 0.30 mmol) in methanol (2 mL) under N_2 were added to a stirred solution of $FeCl_3$ (0.049 g, 0.30 mmol) in methanol (2 mL). After the addition of Et_3N (83.6 μL, 0.60 mmol), the reaction mixture was stirred for 10 min. $NaBPh_4$ (0.10 g, 0.30 mmol) was added to the resulting dark purple blue solution, and the mixture was stirred for 2 h, causing the immediate precipitation of a powder, which was washed with methanol several times and dried in vacuo.

[Fe^{III}((4-MeO)$_2$TPA)(4Cl-cat)]BPh$_4$ (1). Complex **1** was isolated as a gray powder in an 83% yield. ESI-MS: m/z 548.1 ([Fe^{III}((4-MeO)$_2$TPA)(4Cl-cat)]$^+$). Anal. Calcd for $C_{50}H_{45}BClFeN_4O_4$: C, 69.18; H, 5.23; N, 6.45; Cl, 4.08. Found: C, 68.93; H, 5.20; N. 6.45; Cl, 4.07. UV−vis−NIR (CH_3CN, λ_{max}, nm (ϵ, $M^{-1}cm^{-1}$)): 474 (2006), 764 (3038).

[Fe^{III}(TPA)(4Cl-cat)]BPh$_4$ (2). Complex **2** was isolated as a dark blue powder in a 98% yield. ESI-MS: m/z 488.1 ([Fe^{III}(TPA)(4Cl-cat)]$^+$). Anal. Calcd for $C_{48}H_{41}BClFeN_4O_4$: C, 71.35; H, 5.11; N, 6.93; Cl, 4.39. Found: C, 71.21; H, 4.94; N. 6.92; Cl, 4.15. UV−vis−NIR (CH_3CN, λ_{max}, nm (ϵ, $M^{-1}cm^{-1}$)): 483 (1930), 787 (2974).

[Fe^{III}((4-Cl)$_2$TPA)(4Cl-cat)]BPh$_4$ (3). Complex **3** was isolated as a dark blue powder in a 75% yield. ESI-MS: m/z 556.2 ([Fe^{III}((4-Cl)$_2$TPA)(4Cl-cat)]$^+$). Anal. Calcd for $C_{50}H_{45}BClFeN_4O_4$: C, 65.75; H, 4.48; N, 6.39; Cl, 12.13. Found: C, 65.51; H, 4.31; N. 6.41; Cl, 11.87. UV−vis−NIR (CH_3CN, λ_{max}, nm (ϵ, $M^{-1}cm^{-1}$)): 496 (1916), 805 (2953).

[Fe^{III}((4-NO$_2$)TPA)(4Cl-cat)]BPh$_4$ (4). Complex **4** was isolated as a purple powder in a 63% yield. ESI-MS: m/z 533.3 ([Fe^{III}((4-NO$_2$)TPA)(4Cl-cat)]$^+$). Anal. Calcd for $C_{48}H_{42}BClFeN_5O_5$ (**4**·H_2O): C, 65.85; H, 4.86; N, 8.04; Cl, 4.07. Found: C, 65.84; H, 4.78; N. 8.11; Cl, 4.28. UV−vis−NIR (CH_3CN, λ_{max}, nm (ϵ, $M^{-1}cm^{-1}$)): 498 (2038), 815 (2666).

[Fe^{III}((4-NO$_2$)$_2$TPA)(4Cl-cat)]BPh$_4$ (5). Complex **5** was isolated as a purple-blue powder in a 77% yield. ESI-MS: m/z 577.9 ([Fe^{III}((4-NO$_2$)$_2$TPA)(4Cl-cat)]$^+$). Anal. Calcd for $C_{49}H_{43}BClFeN_6O_7$ (**5**·MeOH): C, 63.28; H, 4.66; N, 9.04; Cl, 3.81. Found: C, 63.29; H, 4.55; N. 9.31; Cl, 3.77. UV−vis−NIR (CH_3CN, λ_{max}, nm (ϵ, $M^{-1}cm^{-1}$)): 509 (2408), 856 (1821).

Crystallographic Data Collection and Refinement of the Structure. All measurements were performed on a Rigaku Mercury charge-coupled device with graphite-monochromated Mo Kα (λ

(52) Abbreviations used in this paper are DTBC, 3,5-di-*tert*-butylcatecholate; 4Cl-cat, 4-chlorocatecholate; cat, pyrocatecholate; Cat, catecholate; SQ, semiquinonate; LMCT, ligand-to-metal charge transfer; (4-MeO)$_2$TPA, bis(4-methoxypyridin-2-ylmethyl)(pyridin-2-ylmethyl)amine; TPA, tris(pyridin-2-ylmethyl)amine; (4-Cl)$_2$TPA, bis(4-chloropyridin-2-ylmethyl)(pyridin-2-ylmethyl)amine; (4-NO$_2$)TPA, (4-nitropyridin-2-ylmethyl)bis(pyridin-2-ylmethyl)amine; (4-NO$_2$)$_2$TPA, bis(4-nitropyridin-2-ylmethyl)(pyridin-2-ylmethyl)amine; BLPA, bis((6-methyl-2-pyridyl)methyl)(2-pyridylmethyl)amine; BBA, bis(benzimidazolyl-2-methyl)amine.

(53) Hitomi, Y.; Higuchi, M.; Minami, H.; Tanaka, T.; Funabiki, T. *Chem. Commun.* **2005**, 1758−1760.

(54) Tamura, M.; Urano, Y.; Kikuchi, K.; Higuchi, T.; Hirobe, M.; Nagano, T. *Chem. Pharm. Bull.* **2000**, *48*, 1514−1518.

(55) Gafford, B. G.; Holwerda, R. A. *Inorg. Chem.* **1989**, *28*, 60−66.

Table 1. Crystallographic and Refinement Data for **2**

emprical formula	$C_{48}H_{41}BClFeN_4O_2$
fw	807.99
color	purple
cryst syst	monoclinic
space group	$P2_1/c$ (No. 14)
a (Å)	14.007(2)
b (Å)	9.994(2)
c (Å)	28.419(4)
α (deg)	90
β (deg)	97.396(4)
γ (deg)	90
Z	4
V (Å^3)	3945(1)
D_{calcd} (g cm^{-3})	1.360
μ (cm^{-1})	4.96
temp (K)	243.2
λ(Mo Kα) (Å)	0.71069
no. of reflns	5046
no. of params	514
reflns/params ratio	9.82
GOF	1.141
R_{int}	0.038
R, R_w[b]	0.058, 0.090

[a] $I > 3.0\sigma(I)$. [b] $R = \sum||F_o|-|F_c||/\sum|F_o|$. $R_w = [\sum w(|F_o|-|F_c|)^2/\sum w|F_o|^2]^{1/2}$.

= 0.71069 Å) radiation at 243 K. Crystallographic data are given in Table 1. The structure was solved by standard direct methods (the Crystal-Structure crystallographic software package of the Molecular Structure Corp. and Rigaku). Full-matrix least-squares refinements (SHELXL-97)[56] were carried out with anisotropic thermal parameters for all non-hydrogen atoms.

Physical Methods. Elemental analyses were performed at the Microanalytical Center of Kyoto University. Electrospray ionization mass spectrometry (ESI-MS) spectra were recorded on a PE SCIEX API 2000 mass spectrometer. ^{1}H and ^{13}C NMR spectra of organic compounds and ^{1}H NMR spectra of ferric complexes were recorded on JEOL EX400 and AL300NMR spectrometers, respectively. X-band EPR spectra were recorded at 123 K on a JEOL JES-SRE2X spectrometer. UV−vis−NIR spectra were recorded on either a Hitachi U-3500 or a Photal MCPD-1000 spectrophotometer. Electrochemical studies were performed in a glovebox by using a BAS CV-50W voltammetric analyzer. The solvent, supporting electrolyte, and electrodes are acetonitrile, 0.1 M tetrabutylammonium tetrafluoroborate, and a standard three-electrode system with glassy carbon working electrode, platinum-wire counter electrode, and Ag/Ag$^+$/CH_3CN reference electrode. Magnetic susceptibilities were recorded on a Quantum Design SQUID susceptometer interfaced with a HP Vectra computer system over the temperature range of 5−340 K at the magnetic field of 0.4 T. Since the magnetic behavior in the solid state is generally influenced by not only the substituent effects but also other factors, such as defect, grain boundaries, vacancies, and other imperfections,[57] complexes **1**−**5** were ground with a mortar and pestle to obtain samples under conditions as close to the same as possible. The data were corrected for diamagnetism using Pascal's constants.[58]

Oxygenations of Catecholatoiron(III) Complexes for Product Analysis. The solutions containing complexes **1**−**5** (5 mM) in CH_3CN (5 mL) were stirred under 1 atm of O_2 at 25 °C for 5 h. Aliquots of the reaction solution (2 mL) were diluted with CH_2Cl_2 (2 mL) and washed with 2N HCl to decompose the iron complex. The organic products were extracted with CH_2Cl_2, dried over anhydrous Na_2SO_4, and concentrated in vacuo. The products were quantitatively analyzed by ^{1}H NMR spectroscopy by monitoring specific ^{1}H NMR peaks of products using anthracene as an internal reference.

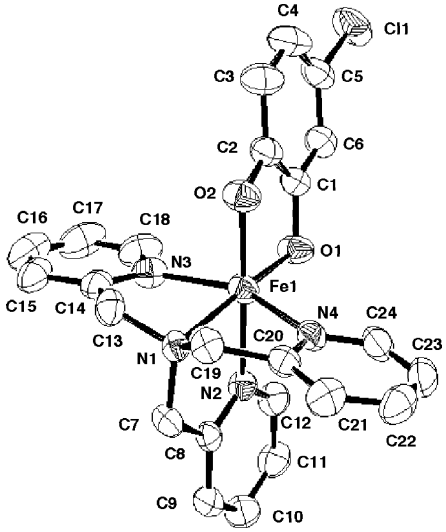

Figure 1. ORTEP plot of the [Fe^{III}(TPA)(4Cl-cat)]$^+$ cation in **2**. Ellipsoids are drawn at the 50% probability level. Hydrogens have been omitted for clarity.

Table 2. Selected Bond Lengths (Å) and Angles (deg) for [Fe^{III}(TPA)(4Cl-cat)]BPh_4 (**2**)

Fe1−O1	1.917(2)	Fe1−N3	2.138(3)
Fe1−O2	1.925(2)	Fe1−N4	2.139(2)
Fe1−N1	2.195(2)	C1−O1	1.352(3)
Fe1−N2	2.114(2)	C2−O2	1.351(3)
N1−Fe1−N2	80.21(8)	O1−Fe1−O2	85.49(8)
N1−Fe1−N3	76.68(9)	O2−Fe1−N3	90.26(9)
N1−Fe1−N4	76.35(8)	O2−Fe1−N4	96.17(9)
N1−Fe1−O2	100.50(8)	N1−Fe1−O1	173.17(9)
O1−Fe1−N2	93.67(8)	N2−Fe1−O2	177.51(9)
O1−Fe1−N3	100.18(10)	N3−Fe1−N4	152.98(9)
O1−Fe1−N4	106.46(9)		

Kinetic Measurements. The solutions containing complexes **1**−**5** (1 mM) were prepared under N_2 in a glovebox. The oxygenation reaction was started by adding the complex solution (0.2 mL) to CH_3CN (3.8 mL), equilibrated at the atmospheric pressure of O_2 at 243 K. The reaction exhibited pseudo-first-order kinetics for all the complex because of the excess of O_2. The pseudo-first-order rate constants were estimated by fitting a decay in the intensity of the lower-energy LMCT band.

Results

X-ray Crystal Structure of [Fe^{III}(TPA)(4Cl-cat)]$^+$. Crystals suitable for X-ray analysis were obtained only with **2**. Figure 1 and Table 2 show an ORTEP plot and selected bond lengths (Å) and dihedral angles (deg) for [Fe^{III}(TPA)-(4Cl-cat)]$^+$, respectively. Compared with the DTBC analogue,[28] the distortion from octahedral geometry is smaller. As for the bond lengths of ligands, the C1−O1/C2−O2, Fe−O1/O2, and Fe−N1/N2 (N1 is aliphatic and N2 is trans to a catecholate oxygen) distances are similar, longer, and shorter, respectively, compared to those of the DTBC complexes (1.349(4)/1.347(4), 1.898(2)/1.917(3), and 2.221(3)/2.145-(3) Å). This indicates that the catecholate dianion coordinates

(56) Sheldrick, G. M. *SHELXL-97, Program for X-ray Crystal Structure Refinement*; University of Göttingen: Göttingen, Germany, 1997
(57) Haddad, M. S.; Federer, W. D.; Lynch, M. W.; Hendrickson, D. N. *J. Am. Chem. Soc.* **1980**, *102*, 1468−1470.
(58) Kahn, O. *Molecular Magnetism*; VCH: New York, 1993.

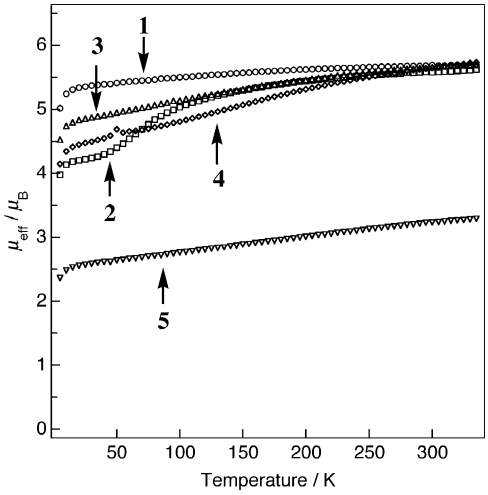

Figure 2. Temperature dependence of the effective magnetic moments for complexes **1**−**5** from SQUID susceptibility measurements.

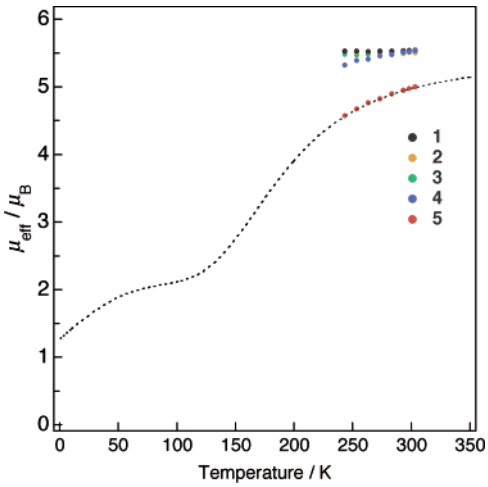

Figure 3. Temperature dependence of the effective magnetic moments for complexes **1**−**5** in CH_3CN from 243 to 303 K. The dotted curve is obtained by the fitting for **5**.

more weakly to the ferric center in the 4Cl-cat complex than in the DTBC complex, while the two TPA nitrogens coordinate more strongly in the former.

Magnetic Susceptibility in the Solid State. Figure 2 shows the temperature dependence of the effective magnetic moment μ_{eff} of **1**−**5** in the solid state. Complexes **1**−**4** exhibited μ_{eff} values of ca. 5.7 μ_B at around 300 K, indicating the high-spin ferric state. The μ_{eff} values decreased to 5.3 μ_B (**1**), 4.2 μ_B (**2**), 4.8 μ_B (**3**), and 4.4 μ_B (**4**) at 15 K, indicating the spin-crossover transition from $S = 5/2$ to $S = 1/2$. On the other hand, the μ_{eff} values of **5** were substantially smaller than those of **1**−**4** and varied from 3.3 μ_B to 2.5 μ_B upon lowering the temperature from 340 to 15 K. The results indicate that **5** contains a large proportion of low-spin species within the temperature range observed. For all complexes, the steep changes in μ_{eff} at 5−15 K may be the result of the zero-field splitting of the high-spin ferric center.

Magnetic Susceptibility in Solution. The magnetic susceptibility of the complexes in CH_3CN was estimated by the Evans method. Figure 3 shows the μ_{eff} values of **1**−**5** at 243−303 K. In this temperature range, the magnetic behavior is similar to that in the solid state. The μ_{eff} values of **1**−**3** were ca. 5.5 μ_B in this temperature range, which are smaller than the 5.9 μ_B value expected for $S = 5/2$. On the other hand, the μ_{eff} values of **4** and **5** decreased from 5.5 to 5.3 μ_B and from 5.0 to 4.6 μ_B, respectively, with lowering temperature, indicating the spin-crossover transition from $S = 5/2$ to $S = 1/2$. The μ_{eff} value of the spin-crossover ferric complex between high-spin and low-spin states is represented by eq 1[59]

$$\mu_{eff}^2 = [\{(1 + 2k)^2/3 + 8(2 + k)^2/9x\} \exp(x) + \{10(1 - k)^2/3 - 8(2 + k)^2/9x\} \exp(-x/2) + 3P\mu_{eff}^{hs\,2} \exp(-E/k_BT)][\exp(x) + 2 \exp(-x/2) + 3P \exp(-E/k_BT)]^{-1} \quad (1)$$

where $x = \zeta'/k_BT$, and k_B denotes the Boltzmann constant, k the orbital reduction factor, ζ' the one-electron spin−orbit coupling constant of the complex, P the ratio of the molecular partition functions of the high- and low-spin states, μ_{eff}^{hs} the effective magnetic moment of the high-spin species, and E the energy separation between zero-point levels of the high-spin and low-spin states. In addition, ζ' is associated with k in the relations $\zeta' = \eta^2\zeta$ and $k = 1/2 + \eta^2/2$,[59] where ζ and η denote the one-electron spin−orbit coupling constant for a free ferric ion and the coefficient of the wave function of the d orbitals, respectively; $\zeta = 460$ cm^{-1}. In case of **5**, the parameters of spin crossover, $P = 90.1 \pm 3.7$ and $E = 646 \pm 7.6$ cm^{-1}, were obtained by fitting the experimental μ_{eff} values to eq 1 using $\zeta' = 110$ cm^{-1}, $k = 0.61$, which was estimated using EPR analysis (vide infra), and $\mu_{eff}^{hs} = 5.50$ μ_B, which is the μ_{eff} value of high-spin ferric complexes **1**−**3**. The fitting curve is shown as a dotted line in Figure 3. Using eq 2, these parameters lead to the Boltzmann distribution of a 64% high-spin state ($f_{^6A}$) and a 36% low-spin state (16% $^2E(f^2_E)$ and 20% $^2A(f^2_A)$, where ^2E and ^2A are the excited and ground-state Kramers doublets, respectively).

$$f_{^6A} = [3P \exp(-E/k_BT)][\exp(x) + 2 \exp(-x/2) + 3P \exp(-E/k_BT)]^{-1}$$

$$f_{^2E} = [2 \exp(-x/2)][\exp(x) + 2 \exp(-x/2) + 3P \exp(-E/k_BT)]^{-1}$$

$$f_{^2A} = [\exp(x)][\exp(x) + 2 \exp(-x/2) + 3P \exp(-E/k_BT)]^{-1} \quad (2)$$

In the case of **4**, sufficient data for parameters were not available to estimate the spin equilibrium. However, it is clear that **4** has only a small contribution of the low-spin species even at 243 K.

Temperature Effects on the Paramagnetic ^{1}H NMR Shifts. Figure 4 shows the ^{1}H NMR spectra of **1**−**5** in CD_3CN at 298 K. The wide and broad spectra indicate that all complexes predominantly have a high-spin ferric center.[27,28,60,61] The proton signals of the TPA and 4Cl-cat ligands

(59) Golding, R. M. *Applied Wave Mechanics*; Van Nostrand Co.: New York, 1969.
(60) Lim, J. H.; Lee, H. J.; Lee, K. B.; Jang, H. G. *Bull. Korean Chem. Soc.* **1997**, *18*, 1166−1172.

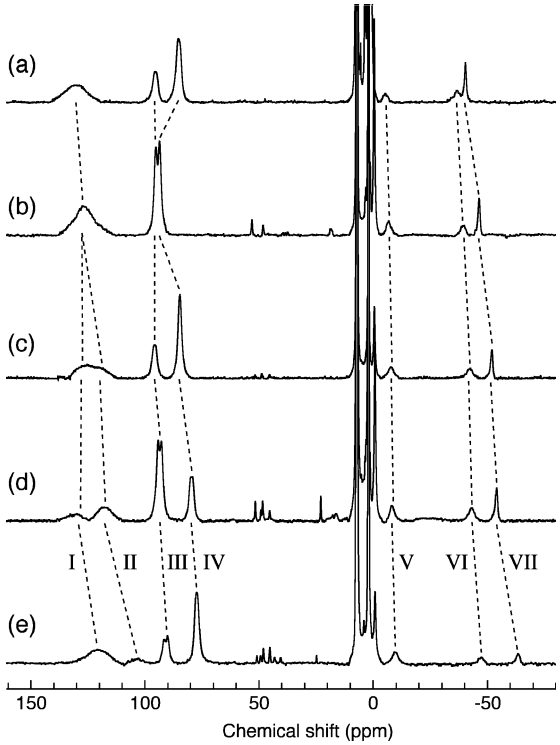

Figure 4. ^{1}H NMR spectra of complexes **1**−**5** in CD_3CN at 298 K: (a) **1**, (b) **2**, (c) **3**, (d) **4**, and (e) **5**. Assignment of H signals are as follows: I, CH_2(R-py); II, CH_2(py); III, β,β'−H (py); IV, β,β'−H (R-py); and V−VII, 3 Hs of 4Cl-cat.

appeared down- and upfield, respectively. With the increasing electron-withdrawing effect of the substituents on the TPA ligand, most of the proton signals were shifted upfield: CH_2 (py) 130 (**1**) → 103 ppm (**5**), β,β'-H (py) 95.5 (**1**) → 90.1 ppm (**5**), β,β'-H (R-py) 85.4 (**1**) → 77.4 ppm (**5**), and CH (4Cl-cat) (−5.5, −36.6, −40.4) (**1**) → (−9.7, −45.5, −63.5) ppm (**5**) (Table S1).

Participation of the low-spin species of **4** and **5** in solution was also studied by variable-temperature ^{1}H NMR measurements. Figure 5 shows the Curie plots of some proton signals of **1**−**5** at 243−303 K. As shown in Figure 5A−C, the proton signals of the TPA ligands of **1**−**3** gave linear plots. The intercept values at $T^{-1} = 0$, which are shown in parentheses in Figure 5, are close to the chemical shifts of free TPA ligands, indicating that the spin-crossover transition does not take place in this temperature range. Complex **4** also gave linear plots, but the intercept values at $T^{-1} = 0$ for β-H deviated greatly from the diamagnetic region (e.g., 19.0, 19.8 ppm), which may result from the spin-crossover transition. Complex **5** showed nonlinear lines, clearly reflecting the spin-crossover transition of **5**. On the other hand, as shown in Figure 5D−F, the temperature dependence of the proton signals of the 4Cl-cat ligands showed linear features but in a different manner than the Curie law. It is very interesting that even **4** and **5** exhibited linear features similar to those of **1**−**3**, despite their spin-crossover transition.

EPR Parameters and Electronic Geometry of Complexes in Solution. Figure 6 shows the EPR spectra of **1**−**5** in frozen CH_3CN at 123 K. This spectral change demonstrates that the proportion of low-spin species increases as the substituents on the TPA ligands become more electron-withdrawing.

EPR parameters (g value and rhombicity (E/D)) for the high-spin species were estimated by the reported method.[62] As shown in Table 3, two sets of g and E/D values were observed with all complexes. Two different E/D values of 0.07−0.08 (major) and 0.13−0.14 (minor) indicate the presence of two different components, probably structural isomers.

The peaks assignable to low-spin species were analyzed by applying the method for axial EPR spectra[59,63,64] to evaluate the spin delocalization between Fe^{III} and ligands. When Hamiltonian (3) is employed for the one-electron orbitals for the t_{2g}^5 configuration, the Zeemann Hamiltonian operators which can be applied to solve a set of three secular equations for the ground-state Kramers doublet are represented by eq 4

$$H = \zeta ls - \delta(l_z^2 - 2/3) - (\epsilon/2)(l_+^2 + l_-^2) \qquad (3)$$

$$g_x = 2[2AC - B^2 + k\sqrt{2}B(C - A)]$$

$$g_y = -2[2AC + B^2 + k\sqrt{2}B(C + A)]$$

$$g_z = -2[k(A^2 - C^2) + A^2 - B^2 + C^2]$$

$$A^2 + B^2 + C^2 = 1 \qquad (4)$$

where ζ, δ, and ϵ, are the one-electron spin−orbit coupling constant, the axial distortion, and the lower symmetry distortion, respectively, A, B, and C are the coefficients characterizing the two spinors of the ground-state Kramers doublet, and k is the orbital reduction factor. Assuming that $C = 0$ for axial EPR spectra, the parameters are represented by eq 5

$$g_\perp = -2[\sin^2\alpha + \sqrt{2}k \sin\alpha \cos\alpha]$$

$$g_{||} = 2[\sin^2\alpha - (1 + k)\cos^2\alpha]$$

$$\delta/\zeta = 2^{-1/2}(\tan\alpha - \cot\alpha + 2^{-1/2})$$

$$\epsilon/\zeta = 0 \qquad (5)$$

where A and B are replaced with cos α and sin α, respectively, on the basis of $A^2 + B^2 = 1$. In this analysis, two sign sets of the g values (i.e., ($g_\perp$, $g_{||}$) = (−, +) and ($g_\perp$, $g_{||}$) = (−, −)) are probable.[64,65] The fitting of the former set to eq 5 leads to a k value of 0.61 and a very small A value (0.093−0.107), a very large B value (0.994−0.996), and a large δ/ζ (7.01−8.01) value. On the other hand, the latter set of g values leads to a k value of 1.06, an A value of 0.801−0.804, a B value of 0.595−0.599, and a δ/ζ value of 0.07−0.08. The k value close to 0.6 for the former set

(61) Yoon, S.; Lee, H. J.; Lee, K. B.; Jang, H. G. *Bull. Korean Chem. Soc.* **2000**, *21*, 923−928.
(62) Wickman, H. H.; Klein, M. P.; Shirley, D. A. *J. Chem. Phys.* **1965**, *42*, 2113−2117.
(63) Griffith, J. S. *The Theory of Transition-Metal Ions*; University Press, Cambridge, U.K., 1961.
(64) DeSimone, R. E. *J. Am. Chem. Soc.* **1973**, *95*, 6238−6244.
(65) McGarvey, B. R. *Coord. Chem. Rev.* **1998**, *170*, 75−92.

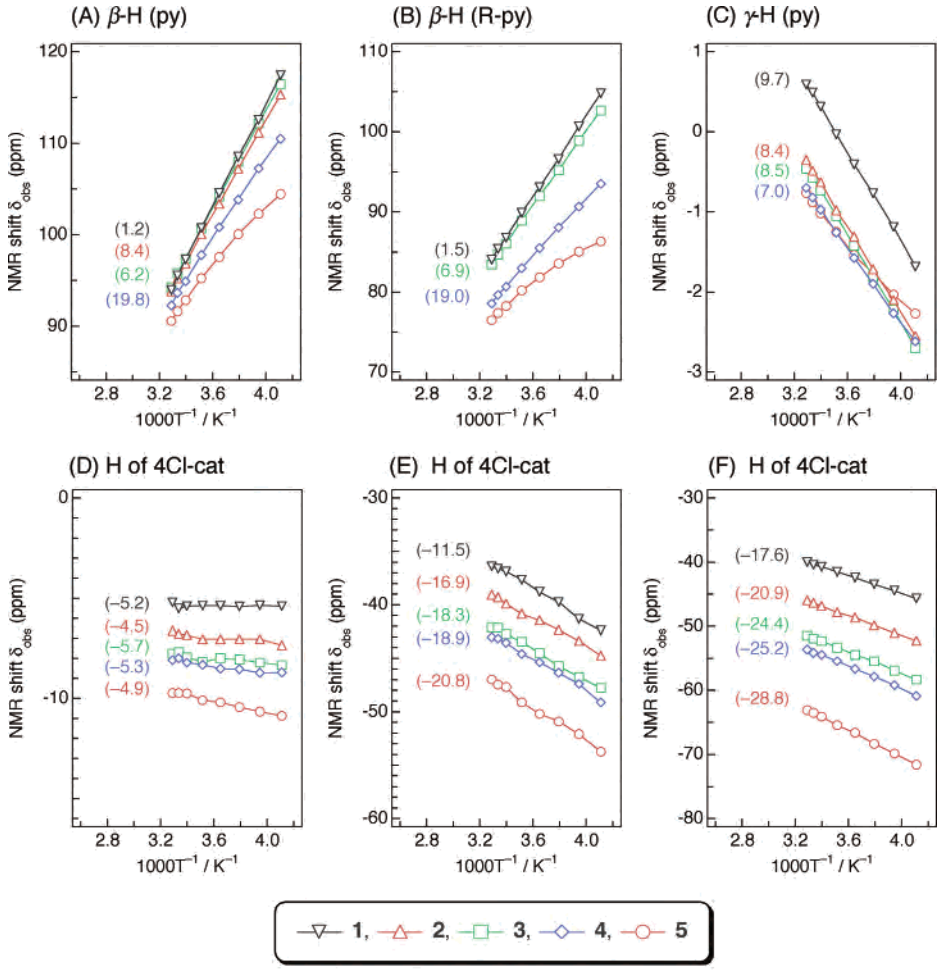

Figure 5. Curie plots for some signals of **1**−**5**: (A) β−H (py), (B) β−H (R-py), (C) γ−H (py), and (D)−(F) 3Hs of the 4Cl-cat ligand. The apparent intercepts at $1000T^{-1} = 0$ are given in parentheses on the left.

theoretically leads to the spin delocalization of 20% low-spin Fe^{III} and 80% ligands in the ground-state Kramers doublet,[59,66] which suggests the low-spin semiquinonatoiron(II) complex as the ground state. Thus, the former set may be excluded because the EPR spectra around $g = 2$ are attributed to low-spin ferric complexes. We however favor the former set because low-spin iron(III)−TPA complexes are expected to have a large δ/ζ because of the t_{2g} orbitals degenerated by interactions between three nitrogen p_π orbitals of the TPA ligand and only one d_π orbital. The k value smaller than 0.75, which is the lower limit expected for the low-spin Fe^{III}−Cat state, is probably obtained because the analysis method used here has been developed for simpler metal complexes, such as porphyrinate and dithiocarbamate complexes.[67] It is still noteworthy, however, that the small k value affords reasonable support for the significant spin delocalization on the 4Cl-cat ligand.

Electrochemical Properties. In the cyclic voltammogram measurements at room temperature, quasi-reversible waves showed cathodic $Fe^{III} \rightarrow Fe^{II}$ (E_{pc}) and anodic $Cat^{2-} \rightarrow SQ^{\bullet-}$ (E_{pa}) wave peaks. As shown in Table 4, the E_{pc} of Fe^{III}/Fe^{II} was dependent on the substituents on the TPA ligand and varied from −903 (**1**) to −641 mV (**5**), whereas the E_{pa} of $SQ^{\bullet-}/Cat^{2-}$ was not sensitive to the substituents in the range of 198−228 mV. This result suggests that the substituents of the TPA ligand influence the d-orbital energy of the ferric center but not the orbital energy of the 4Cl-cat ligand.

LMCT Bands in UV−vis−NIR Spectroscopy. As shown in Table 4 and Figure S1, complexes **1**−**5** in CH_3CN exhibited two intense LMCT bands (λ_1 and λ_2) characteristic of catecholatoiron(III) complexes.[19,68,69] The electron-withdrawing substituents on the TPA ligand brought about red shifts of both λ_1 and λ_2. As for the peak intensity, **5** exhibited unique spectra, $\epsilon_1 > \epsilon_2$, whereas $\epsilon_1 < \epsilon_2$ for **1**−**4**. Because this characteristic feature was thought to be caused by the low-spin fraction, the temperature effect on the spectra was studied by lowering the temperature from 303 to 243 K. Complexes **1**−**3** exhibited no effect on the intensities of the λ_1 and λ_2 bands but showed slight blue shifts with isosbestic points (Figure 7A for **2**, Figure S2 for **1** and **3**). On the other hand, **5** exhibited spectral changes with an increase in the intensity of λ_1 and with a decrease in the intensity and blue shift of the λ_2 band. In addition, the spectral

(66) Stevens, K. W. H. *Proc. R. Soc. London A* **1953**, *219*, 542−555.
(67) Rieger, P. H. *Coord. Chem. Rev.* **1994**, *135*, 203−286.
(68) Cox, D. D.; Benkovic, S. J.; Bloom, L. M.; Bradley, F. C.; Nelson, M. J.; Que, L., Jr.; Wallick, D. E. *J. Am. Chem. Soc.* **1988**, *110*, 2026−2032.
(69) Dei, A.; Gatteschi, D.; Pardi, L. *Inorg. Chem.* **1993**, *32*, 1389−1395.

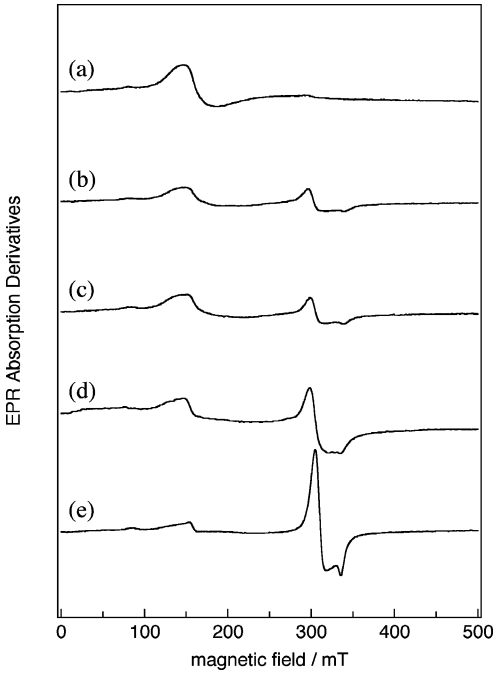

Figure 6. X-band EPR spectra recorded in CH_3CN at 123 K. The EPR conditions are microwave frequency, 9.06 kHz; microwave power, 20 mW; modulation amplitude, 1 mT; and modulation frequency, 100 kHz: (a) **1**, (b) **2**, (c) **3**, (d) **4**, and (e) **5**.

change in **5** was accompanied by the growth of new peaks at around 1100 nm. Complex **4** exhibited a mixture of the above two types of spectral changes, with smaller peaks at around 1100 nm than those of **5**. The lowest-energy peaks could be assigned to the LMCT bands of low-spin species.[34]

Reactivity of the Complexes with Molecular Oxygen. The reaction of **1**−**5** with O_2 in CH_3CN afforded exclusively *cis*-dienelactone, which is produced by the intradiol oxygenation of the 4Cl-cat ligand followed by dechlorination of the muconic anhydride.[70]

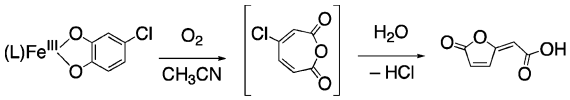

(6)

To elucidate the effect of the ligand substituents on the reactivity with O_2, we estimated the reaction rates by monitoring the decay of the lower-energy LMCT band (λ_2) (Figure S3).[70] The oxygenation rate constant, k_{obs}, was obtained under the conditions of pseudo-first-order kinetics. As shown in Table 4, k_{obs} increased in the order of **1** < **2** < **3** < **4** < **5**.

Discussion

In the developments in bioinorganic chemistry involving the catechol dioxygenases and their model systems, the formation of the high-spin catecholatoiron(III) complex as an intermediate and the participation of the semiquinonatoiron(II) form have become well accepted to explain the reaction mechanisms. However, there have been discussions for a long time on how the high-spin catecholatoiron(III) complex reacts with O_2. To provide insight into the reaction mechanism, we prepared an admixture of high- and low-spin catecholatoiron(III) complexes in solution. Although the low-spin complexes are not regarded as models for high-spin catechol dioxygenases, the reactivity of the low-spin catecholatoiron(III) species with O_2 is expected to provide important information about the reaction mechanisms of the high-spin species. Scheme 2 summarizes the relationship among spin crossover, spin delocalization, and the reaction of the complexes with O_2.

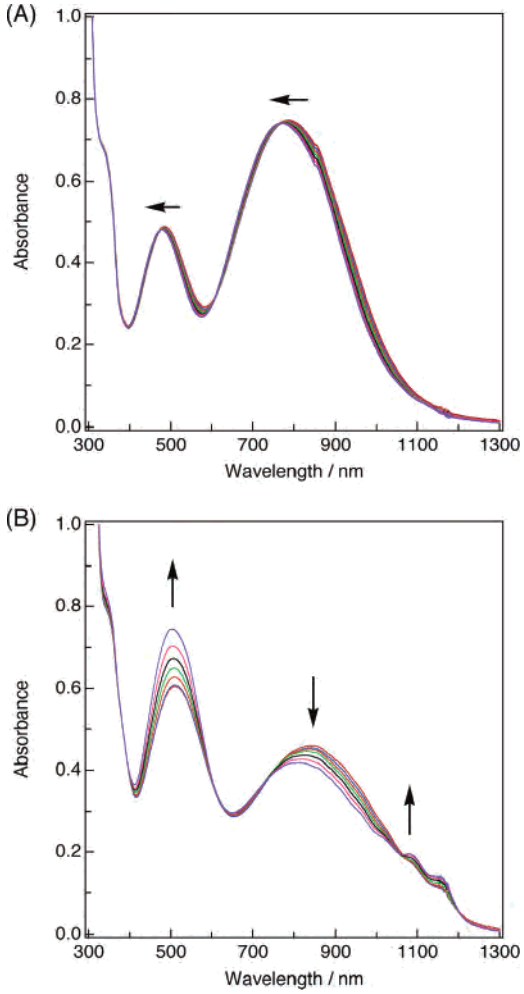

Figure 7. Variable-temperature UV−vis−NIR spectra for (A) **2** and (B) **5** at 298, 293, 283, 273, 263, 253, and 243 K. The arrows represent changes on going to lower temperature.

Admixture of High- and Low-Spin Catecholatoiron(III) Complexes, (*i*). The ^1H NMR spectra at 298 K show the substituent effects of the TPA ligand. Both the TPA and 4Cl-cat protons are shifted upfield as the substituents become more electron-withdrawing. The upfield shifts of the TPA protons indicate that the interactions of the TPA ligand with e_g orbitals of the ferric ion become less effective because the TPA protons appear in the downfield region as a result of a σ-spin delocalization mechanism via the e_g orbitals. On the other hand, because the 4Cl-cat protons appear in the upfield region as a result of a π-spin delocalization mechanism via the t_{2g} orbitals, the upfield shifts of the 4Cl-cat

(70) Funabiki, T.; Yamazaki, T.; Fukui, A.; Tanaka, T.; Yoshida, S. *Angew. Chem., Int. Ed.* **1998**, *37*, 513−515.

Table 3. Experimental EPR Parameters for High-Spin and Low-Spin Species of **1**−**5** at 123 K

	high-spin	low-spin						
	g values (*E*/*D*)	$g_\perp$ value	$g_\parallel$ value	Σg^2	cos α	sin α	*k*	δ/ζ
1	8.5 (0.13); 7.7, 4.1 (0.08)	−2.160	—[a]	—[b]	—[b]	—[b]	—[b]	—[b]
2	8.6 (0.14); 7.6, 4.3 (0.07)	−2.167	1.940	13.16	0.107	0.994	0.63	7.01
		−2.167	−1.940	13.16	0.801	0.599	1.07	0.08
3	8.6 (0.14); 7.3, 4.2 (0.07)	−2.160	1.941	13.10	0.106	0.994	0.61	7.04
		−2.160	−1.941	13.10	0.802	0.598	1.07	0.08
4	8.5 (0.13); 7.3, 4.2 (0.07)	−2.153	1.945	13.05	0.103	0.995	0.60	7.27
		−2.153	−1.945	13.05	0.802	0.597	1.06	0.08
5	8.5 (0.13); 7.3, 4.2 (0.07)	−2.141	1.955	12.99	0.093	0.996	0.61	8.01
		−2.141	−1.955	12.99	0.804	0.595	1.06	0.07

[a] Not determined because of a broad EPR spectrum for **1**. [b] Not calculated because there was no observation of $g_\parallel$.

Table 4. Spectroscopic and Kinetics Data for **1**−**5** in CH_3CN

			potential[c] (mV)		
complex	μ_{eff}[a] (μ_B)	λ_1, λ_2[b] (nm) (ϵ_1, ϵ_2 ($M^{-1}cm^{-1}$))	$E_{pc}(Fe^{III}/Fe^{II})$	$E_{pa}(SQ^{\bullet -}/Cat^{2-})$	k_{obs}[a] ($\times 10^{-4}$ s^{-1})
1	5.5	474 (2010), 767 (3040)	−903	228	0.18
2	5.5	483 (1930), 787 (2970)	−828	198	0.67
3	5.5	496 (1920), 805 (2950)	−748	203	1.6
4	5.3	498 (2040), 815 (2670)	−731	198	2.1
5	4.6	509 (2410), 839 (1820)[d]	−641	228	2.9

[a] Measured at 243 K. [b] Measured at 298 K. [c] Measured at room temperature. All the *E* values are referenced to the Fc/Fc^+ couple. Conditions were a scan rate of 100 mV/s, under ambient temperature and N_2. E_{pc} and E_{pa} show cathodic and anodic potential, respectively. [d] Other peaks observed, λ (ϵ): 1090 (640), 1160 (400).

Scheme 2

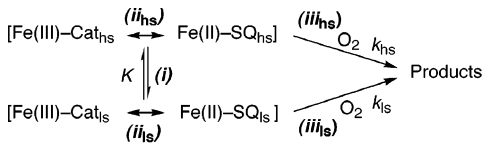

protons indicate that the interactions of the 4Cl-cat ligand with t_{2g} orbitals of the ferric ion become more effective. Weak coordination of the TPA ligand with electron-withdrawing substituents should stabilize both e_g and t_{2g} orbitals, which take into account the respective upfield shifts of the TPA and 4Cl-cat protons. The effective induction of low-spin species with electron-withdrawing substituents indicates greater stabilization of the t_{2g} orbital than the e_g orbital because it leads to a larger crystal-field splitting.

The admixture of two spin states in the solid state was clearly shown by measurement of the magnetic susceptibility. As shown in Figure 2, complexes **1**−**4** are in the high-spin state with μ_{eff} = ca. 5.7 μ_B at around room temperature, and they exhibit spin-crossover behavior with decreasing temperature. This μ_{eff} value smaller than 5.9 μ_B, which is expected from ferric complexes in the fully $S = 5/2$ ground state, may be the result of the spin delocalization on the ligand, the existence of intermolecular magnetic interactions, or both.[51,57,71] Remarkably, complex **5** is in the admixture state even at room temperature (μ_{eff} = 3.3 μ_B), indicating the strong substituent effect of the two NO_2 groups on the crystal field parameter.

The admixture in solution was shown by measurements of the magnetic susceptibility, ^1H NMR, EPR, and UV−vis−NIR spectra. The μ_{eff} values of **1**−**3**, estimated by the Evans method at 243−303 K, are 5.5 μ_B, indicating that complexes **1**−**3** do not show spin crossover behavior in this temperature range and are in the high-spin state. This result is also consistent with the chemical shifts in the diamagnetic region at $T^{-1} = 0$ in the linear Curie plots of ^1H NMR signals of the TPA ligand (Figure 5A−C). In the case of complex **5**, the μ_{eff} value varies from 4.6 μ_B (243 K) to 5.0 μ_B (303 K). The proportion of the high-spin species is estimated to be 64% at 243 K by simulation of the observed data using μ_{eff}^{hs} = 5.5 μ_B. The nonlinear Curie plots of the TPA protons, as shown in Figure 5A−C, can be accounted for by the spin admixture in **5**. The ^1H NMR shifts of the metal complex in spin equilibrium are represented by a weighted average of the signals for high- and low-spin species in eq 7

$$\delta_{obs} = \delta_{dia} + (1 - x)\delta_{iso}^{hs} + x\delta_{iso}^{ls} \qquad (7)$$

where *x* is the portion of the low-spin species and δ_{obs}, δ_{dia}, δ_{iso}^{hs}, and δ_{iso}^{ls} are the observed, diamagnetic, and isotropic shifts of the high-spin and low-spin complexes, respectively. These nonlinear Curie plots (i.e., the negative deviation of δ_{obs} of the TPA protons from the expected linear plots at the lower temperatures, despite the increase in the *x* value) can be attributed to $\delta_{iso}^{ls} < \delta_{iso}^{hs}$ for the TPA protons. The large downfield shifts of the TPA protons are mainly the result of the σ-spin delocalization;[72] therefore, the relation of $\delta_{iso}^{ls} < \delta_{iso}^{hs}$ reflects the smaller spin number in the e_g orbitals of the low-spin ferric complex. Examples are found for the decrease in isotropic shift caused by the decrease in the spin number in e_g orbitals (e.g., iron(III) dithiocarbamates

(71) Heistand, R. H., II; Lauffer, R. B.; Fikrig, E.; Que, L., Jr. *J. Am. Chem. Soc.* **1982**, *104*, 2789−2796.

(72) Que, L., Jr., Ed. *Physical Methods in Bioinorganic Chemistry: Spectroscopy and Magnetism*; University Science Books: Sausalito, CA, 2000.

in the equilibrium between $S = 5/2$ and $1/2$[73,74] and iron(III) porphyrinates in the equilibrium between $S = 3/2$ and $1/2$).[75] EPR spectra provide a clear support for the admixture caused by the substituent effects. Figure 6 shows that the proportion of low-spin species increases in the order of **1** < **2** ≈ **3** < **4** < **5** at 123 K. UV−vis−NIR spectra also offer support for the admixture at 243−303 K. All complexes exhibit two characteristic peaks of the LMCT band, λ_1 and λ_2 ($\lambda_1 > \lambda_2$ in energy). The intensities of the bands of high-spin complexes **1**−**4** are $\epsilon_1 < \epsilon_2$, but that of **5** is uniquely $\epsilon_1 > \epsilon_2$. As shown in Figure 7B, the intensities of the bands of **5** decrease with decreasing temperature, in harmony with the other spectroscopic supports for the increase in low-spin species at lower temperatures. In addition, new peaks at around 1100 nm grow with decreasing temperature, which may be responsible for progression coupled to the LMCT for low-spin species, as observed for low-spin [Fe(TPA)(cat)]BPh_4 in the solid state.[34]

Semiquinone Character in the High-Spin Complex: Spin Delocalization on the 4Cl-cat Ligand, (*ii*$_{hs}$). The ground state of catecholatoiron(III) complexes is represented as the quantum mechanical admixture of Fe^{III}−Cat and Fe^{II}−SQ states. This means that the ground state Ψ_- and the excited state Ψ_+ of the catecholatoiron(III) complex are represented by

$$\Psi_- = \Psi_{Fe^{III}-Cat} + \alpha\Psi_{Fe^{II}-SQ} \quad (8)$$

$$\Psi_+ = \Psi_{Fe^{II}-SQ} - \alpha\Psi_{Fe^{III}-Cat} \quad (9)$$

$$\alpha = H_{in}/\Delta E \quad (10)$$

where $\Psi_{Fe^{III}-Cat}$ and $\Psi_{Fe^{II}-SQ}$ are the wave functions of the pure Fe^{III}−Cat and Fe^{II}−SQ states, respectively. H_{in} and ΔE denote the charge-transfer integral and the energy difference between the two pure states, respectively (Figure S4). On the other hand, the chemical shift of paramagnetic metal complexes is represented by eq 11

$$\delta_{obs} = \delta_{dia} + \delta_{iso} \quad (11)$$

where δ_{iso} are the isotropic shifts. From a comparison of the relative terms of eq 8 with eq 11, it is clear that δ_{iso} of the 4Cl-cat protons corresponds to $\alpha\Psi_{Fe^{II}-SQ}$ and is an index of the semiquinone character of a catecholate ligand in the ground state.

As shown in Figure 4, the upfield shifts of the 4Cl-cat protons are ascribed to the π-spin delocalization on the 4Cl-cat ligand via LMCT but not to the σ-spin delocalization.[72] For the high-spin ferric complexes **1**−**3**, the increase in the magnitude of δ_{iso} of the 4Cl-cat protons in the order of **1** < **2** < **3** indicates the greater semiquinone character of the catecholate ligand in this order. In addition, as shown in Figure 5D−F, although complexes **1**−**3** remain in the high-spin state, the intercept values of the 4Cl-cat protons of these complexes at $T^{-1} = 0$ are observed in the nondiamagnetic region of −4.9 to −24.4 ppm. A similar non-Curie-law temperature dependence has been observed for the 4-H and 6-H proton signals of the DTBC ligand of [Fe^{III}(BLPA)-DTBC]BPh_4,[69] [Fe^{III}(BBA)DTBC]BPh_4,[61] and [Fe^{III}(TPA)-DTBC]BPh_4.[76] The explanation for iron(III) meso-substituted porphyrinates[77,78] may be applied to this non-Curie-law behavior (i.e., the participation of thermally accessible plural excited states in the catecholate-to-iron charge transfer).

Semiquinone Character in the Low-Spin Complex: Spin Delocalization on the 4Cl-cat Ligand, (*ii*$_{ls}$). It is very interesting and important to determine the spin delocalization in the low-spin catecholatoiron(III) complexes. The EPR spectra in Figure 6 indicate the increasing tendency of the low-spin complexes, **1** < **2** ≈ **3** < **4** < **5**. Analysis of the low-spin peaks of complexes **2**−**5** by the method for axial EPR spectra results in a small value of the orbital reduction factor k (0.61), which represents the significant spin delocalization on the ligands in the low-spin catecholatoiron(III) complex. As for the 4Cl-cat ligand, this was supported by the observation of LMCT bands in the significant low-energy region (i.e., at around 1100 nm).[34]

As shown in Figure 5D−F, the 4Cl-cat protons of spin-crossover complexes **4** and **5** exhibit a non-Curie-law plot similar to that of high-spin complexes **1**−**3**. The linear feature, despite the increasing proportion of the low-spin species at lower temperatures, indicates that the absolute value of δ_{iso} for the low-spin complex is at least not smaller than that of the high-spin analogues: $|\delta_{iso}^{ls}| \geq |\delta_{iso}^{hs}|$ in eq 7, although $\delta_{iso}^{ls} < \delta_{iso}^{hs}$ for the TPA protons. Thus, the change in the d-orbital spin configuration from $e_g^2t_{2g}^3$ to $e_g^0t_{2g}^5$ may be effective in increasing the $d_\pi-p_\pi$ overlap interaction between the ferric center and the 4Cl-cat ligand, resulting in an increase in H_{in}. In addition, the observation of a LMCT band in the low-spin species lower than that in the high-spin analogues shows that the ΔE of the low-spin species is smaller than that of the high-spin analogues. Thus, both the increase in H_{in} and the decrease in ΔE of the low-spin species relative to the high-spin analogues should result in an increase in the α value (i.e., the stronger contribution of the Fe^{II}−SQ state in the low-spin species).

Reactivity of Catecholatoiron(III) Complexes, (*iii*$_{hs}$) and (*iii*$_{ls}$). The oxygenation of catechols catalyzed by iron-containing catechol dioxygenases and model complexes proceeds as follows: (1) the catechol binds to iron to form a catecholatoiron(III) complex, (2) oxygen binds to the catecholatoiron(III) complex, (3) oxygen inserts into the C−C bond of the aromatic ring, (4) the monooxygenated product is hydrolyzed, and 5) the oxygenated product is eliminated to regenerate the iron active species. For step 1, many catecholatoiron(III) complexes which are reactive with O_2 have been developed. For step 2, two processes have been proposed as shown in Scheme 1, but no direct evidence for

(73) Golding, R. M.; Tennant, W. C.; Kanekar, C. R.; Martin, R. L.; White, A. H. *J. Chem. Phys.* **1966**, *45*, 2688−2693.
(74) Golding, R. M.; Tennant, W. C.; Bailey, J. P. M.; Hudson, A. *J. Chem. Phys.* **1968**, *48*, 764−771.
(75) Ikeue, T.; Ohgo, Y.; Ongayi, O.; Vicente, M. G. H.; Nakamura, M. *Inorg. Chem.* **2003**, *42*, 5560−5571.
(76) Higuchi, M.; Hitomi, Y.; Tanaka, T.; Funabiki, T. Unpublished data.
(77) Shokhirev, N. V.; Walker, F. A. *J. Phys. Chem.* **1995**, *99*, 17795−17804.
(78) Banci, L.; Bertini, I.; Luchinat, C.; Pierattelli, R.; Shokhirev, N. V.; Walker, F. A. *J. Am. Chem. Soc.* **1998**, *120*, 8472−8479.

the structure of the O_2 adduct has been obtained.[41,61] For step 3, a reaction via a Criegee[79] or epoxide-type intermediate[33] has been proposed, but details have not been clarified. Present results are valuable for discussions on step 2.

Many catecholatoiron(III) complexes have been synthesized as model complexes for catechol dioxygenases to understand the mechanisms of the oxygenation reaction.[4,22,80] The importance of the semiquinonatoiron(II) character in the catecholatoiron(III) complex has been proposed from the early stage of the model studies.[19,23,39,68,81] In efforts to clarify the mechanism of O_2-binding to the catecholatoiron(III) complex, correlations have been studied between the reactivities and physical properties of these model complexes, such as the energy of the LMCT band,[27−31] the redox potential,[30,31] and the NMR shift of the catecholate proton.[27−29] In these studies, the reactivity was compared with the rate constants of the reactions of the complexes with O_2, although the logarithm of the rate constants is thought to be appropriate for discussions on the basis of the kinetic energies. Recently, we have reported a linear correlation between the logarithm of the rate constants and the energy of the lower-energy LMCT band in the oxygenation of a series of [Fe^{III}(TPA)-(R−Cat)]BPh_4 complexes with substituted Cat ligands.[26]

In this study, the logarithm of the rate constants was plotted against the energy of the lower-energy LMCT band assignable to the high-spin species (Figure 8A). As expected, high-spin complexes **1**−**3** exhibit good linear correlations, supporting the belief that the reactivity of the complexes with O_2 is directly correlated with the Fe^{II}−SQ state.[26] Complexes **4** and **5** show a negative deviation from the linear line, indicating that the low-spin species have lower reactivity than the high-spin analogues. The rate constant for the high-spin species of **5** can be estimated to $k_{hs}[O_2] = 4.30 \times 10^{-4}$ s^{-1} on the basis of the extrapolation of the linear line from the high-spin LMCT energy of **5** in Figure 8A because the negative deviation from the linear correlation is the result of the admixture of the low-spin species. Assuming that both the high- and low-spin species react with O_2, the rate constant of the low-spin species can be estimated to be $k_{ls}[O_2] = 0.41 \times 10^{-4}$ s^{-1} using the values of $k_{obs}[O_2] = 2.90 \times 10^{-4}$ s^{-1}, $k_{hs}[O_2] = 4.30 \times 10^{-4}$ s^{-1}, which is calculated by the linear correlation in Figure 8A, and the equilibrium constant $K =$ 0.56 at 243 K. Thus, this result indicates that the reactivity of the low-spin species is much lower than that of the high-spin analogues.

We have suggested that O_2 attacks the ferric center of the catecholatoiron(III) complex,[26] although the interaction of an iron(III) center with O_2 has been little known, in contrast to the well-known O_2 binding to an iron(II) center. Recently, however, Collins and co-workers demonstrated that the Fe(III)−TAML complex can react with O_2 to yield a μ-oxo-diiron(IV) complex.[82] Thus, a direct O_2 attack on the ferric center may be possible in certain cases (e.g., in the case

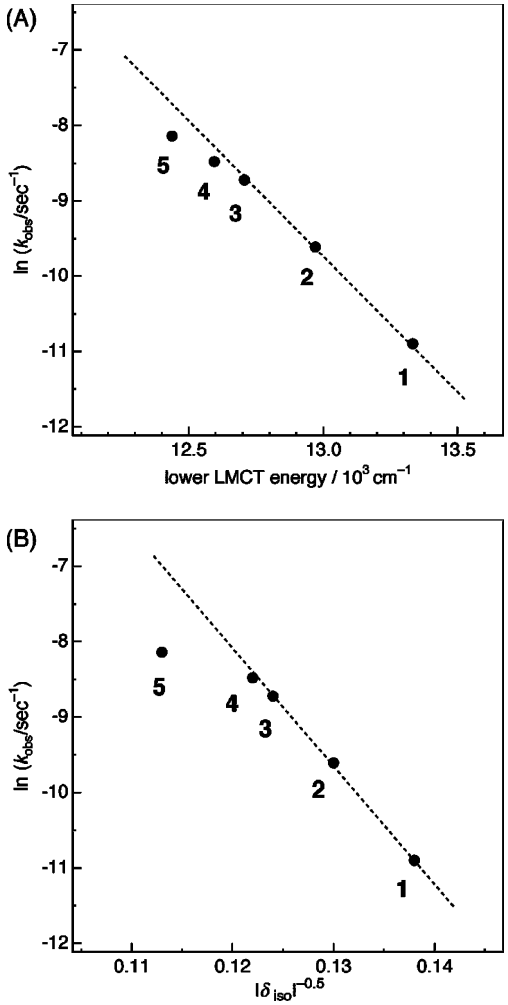

Figure 8. Correlation between ln k_{obs} and the lower-LMCT energy at 243 K (A) and between ln k_{obs} and the NMR shift ($|\delta_{iso}|^{-0.5}$) of the 4Cl-cat proton at 243 K (B). The dotted line represents the linear relationship between **1**−**3**.

where a stable O_2 adduct can be formed). Although the spin-state-dependent reactivity has been known in other iron systems,[83−86] it is still unclear why the low-spin catecholatoiron(III) species has a lower O_2 reactivity than the high-spin species.

The isotropic shift controls mainly the contact shift when the protons are sufficiently distant from the metal center. Thus, as shown in eq 12, δ_{iso} for high-spin ferric complexes is directly proportional to the unpaired-electron spin density, ρ_C, in the p_π orbital of the carbon to which the proton is attached

$$\delta_{iso} = -\frac{Q_{CH}\rho_C h}{2S}\left(\frac{\gamma_e}{\gamma_N}\right)\frac{S(S+1)}{3k_B T} \qquad (12)$$

where S (5/2), h, and Q_{CH} denote the effective spin for the high-spin ferric ion, the Plank constant, and the McConnel

(79) Mayer, R. J.; Que, L., Jr. *J. Biol. Chem.* **1984**, *259*, 13056−13060.
(80) Funabiki, T. *Oxygenases and Model Systems*; Kluwer Academic Publishers: Dordrecht, The Netherlands, 1997; Vol. 19.
(81) Funabiki, T.; Mizoguchi, A.; Sugimoto, T.; Yoshida, S. *Chem. Lett.* **1983**, 917−920.
(82) Ghosh, A.; de Oliveira, F. T.; Yano, T.; Nishioka, T.; Beach, E. S.; Kinoshita, I.; Münck, E.; Ryabov, A. D.; Horwitz, C. P.; Collins, T. J. *J. Am. Chem. Soc.* **2005**, *127*, 2505−2513.
(83) Jensen, K. P.; Ryde, U. *J. Biol. Chem.* **2004**, *279*, 14561−14569.
(84) Shiota, Y.; Yoshizawa, K. *J. Chem. Phys.* **2003**, *118*, 5872−5879.
(85) Franzen, S. *Proc. Natl. Acad. Sci. U.S.A.* **2002**, *99*, 16754−16759.

constant, respectively. Because the spin density, ρ_C, is represented by $\rho_C \propto \alpha^2 = (H_{in}/\Delta E)^2$,[77] $|\delta_{iso}|^{-0.5}$ is proportional to ΔE in the case where H_{in} is constant for the high-spin complexes. Because ΔE can be regarded as the LMCT energy,[87] the plot of ln k_{obs} against $|\delta_{iso}|^{-0.5}$ is also expected to exhibit a linear correlation similar to the plot of ln k_{obs} against the LMCT energy. Indeed, as shown in Figure 8B, the linear correlation was found for high-spin complexes **1**−**3**. Again, this plot also indicates that low-spin complexes have lower reactivity than their high-spin analogues.

Conclusion

We evaluated the spin delocalization on the catecholate ligands by the isotropic shifts of the catecholate protons and found that the semiquinonatoiron(II) character is more significant in the low-spin species than in the high-spin species. The higher semiquinonatoiron(II) character in the low-spin species is also supported by the LMCT band observed at around 1100 nm for the low-spin species. Although a linear relationship between the spin delocalization and the logarithm of the reaction rate of the catecholatoiron(III) complexes with O_2 for the high-spin species, the complexes containing low-spin species negatively deviate from the above linear correlation line, despite their higher semiquinonate character. This finding suggests a crucial role of the iron(III) center in the reaction of the catecholatoiron(III) complexes with O_2. The detailed reaction mechanism is under investigation in our laboratory.

Acknowledgment. We are grateful to Prof. S. Kitagawa and Dr H.-C. Chang for their assistance with the X-ray crystallographic analysis. Prof. M. Kodera provided useful advice. This work was financially supported by a Grant-in-Aid for Scientific Research (No. 14750679) from the Ministry of Education, Science, Sports, and Culture, Japan. Y.H. is grateful to the Mizuho Foundation for the Promotion of Sciences for financial support.

Supporting Information Available: The NMR shifts of complexes **1**−**5** at 298 K (Table S1), UV−vis−NIR spectra for **1**−**5** at 298 K (Figure S1), variable-temperature UV−vis−NIR spectra for **1**, **3**, and **4** at 243−303 K (Figure S2), progress of the oxygenation reaction of **2** at 243 K (Figure S3), potential surface for the charge-transfer complex (Figure S4), and X-ray crystallographic data for **2** in CIF format. This material is available free of charge via the Internet at http://pubs.acs.org.

IC051173Y

(86) Bassan, A.; Blomberg, M. R. A.; Siegbahn, P. E. M.; Que, L. *J. Am. Chem. Soc.* **2002**, *124*, 11056−11063.
(87) Foster, R. *Organic Charge-Transfer Complexes*; Academic Press: New York, 1969.